ISSN 1330-3651 (Print), ISSN 1848-6339 (Online) https://doi.org/10.17559/TV-20240430001510
Original scientific paper

ESO Based MPC Design and Experiment Investigation for a Fin Stabilizer Electro-Hydraulic Servo System

Jiguang SONG, Yanxin LIU, Jingfu WANG*, Lihua LIANG

Abstract: In the present study, an extended state observer-based model predictive controller was designed to enhance the response rate and disturbance rejection of the fin electro-hydraulic servo system without overshoot and extend the application of fin stabilizer at zero speed. To this end, a tracking differentiator was employed to implement the command plan of the fin servo system to limit the overshoot. Moreover, an extended states observer was used to estimate the external disturbance, uncertainty and nonlinearity in the electro-hydraulic servo system. Then, the estimated lumped disturbance was compensated directly in the control command generated by the model predictive control. Accordingly, the response speed and disturbance rejection were designed through the objective function in the predictive control model. Then an electro-hydraulic servo system of a fin stabilizer was studied to evaluate the performance of the proposed control strategy. The experimental results revealed that the proposed controller improved the response speed and disturbance rejection capacity of electro-hydraulic servo system of fin. The improved control strategy can adapt well to the requirements of zero-speed fin stabilizer.

Keywords: electro-hydraulic servo system; model predictive control; rapid response without overshoot; servo system test

1 INTRODUCTION

Electro-hydraulic servo system (EHSS) has superior characteristics, including fast responses and large stiffness and a high power-to-weight ratio [1, 2]. Accordingly, these systems have been widely employed in applications with heavy loads and large inertia. Therefore, EHSS plays an important role in different applications such as robots [3-5], vehicles [6], aircraft [7], and ships [8]. However, studies show that external disturbances, high orders, uncertainties, nonlinearities and complexities accompanied with the EHSS are the main challenges to improve the position precision and robustness through conventional controllers.

In this regard, numerous control strategies have been proposed to improve the control precision and robustness of EHSS. Li combined the artificial neural network and fuzzy logic, then the control precision and the frequency range have improved significantly [6]. Thomas proposed a sliding controller to overcome uncertainties and nonlinearities originating from internal leakages and nonlinear frictions [9]. Wei adopted a fuzzy variable structure controller for coupling parameters and nonlinearity of the hydraulic cylinder [10]. Moreover, Guo established a model with block-strict feedback to avoid the reduction of model orders in an electro-hydraulic system [11]. Then an adaptive controller was employed to overcome the external load and parametric uncertainties. Chaudhuri designed a recurrent Hermite network-based sliding mode control for electric hydraulic positioning systems [12]. Peng used a fuzzy PID control strategy based on a multiply object function for a six-DOF electric hydraulic robot [13]. Furthermore, Lee designed a robust compliance controller with a two-loop structure for an electro-hydraulic robot manipulator to avoid the instability of actuators [14].

Reviewing the literature indicates that the control accuracy and robustness of EHSS have improved recently. However, it is still a challenge to control EHSS precisely at problems with large inertia, strong external disturbance and high uncertainty.

Currently, EHSS is usually employed to drive the fin movement according to the control law. Therefore, a stable moment can be generated by fins, which can be applied to overcome the disturbance moment originating from the wind and ocean waves [15]. Studies show that the pump-controlled EHSS has high efficiency and large load rigidity. Accordingly, it has been widely applied in medium to high-power fin stabilizer servo systems. However, the pump-controlled EHSS has some disadvantages, including lower response speed than the valve-controlled EHSS [16]. The following performance requirements are put forward for the EHSS of fin stabilizers with application of fin stabilizers at zero speed:

(1) The fast flapping mechanism that resembles the step motion is used to generate a stable moment at zero speed. To this end, EHSS should have a rapid response [17].

(2) The working angle is set as large as possible to generate enough force at zero speed. To this end, the fin angle should have no overshoot to prevent the rocker arm of the fin from colliding with the mechanical limiter.

(3) The fin should stop at the position parallel to the streamline angle of the ship to reduce the sailing resistance when the fin stops working. In this regard, the fin EHSS should provide a good position accuracy.

(4) The EHSS is required to provide a large flow rate with low load pressure that decreases the system stiffness. However, there exists a large nonlinear friction torque between the fin shaft and the hull when the fin sustains the stochastic distribution force coming from ocean waves. Then, the precision and stability of the EHSS decrease.

Considering the requirements of stationary fin EHSS, the model predictive control (MPC) strategy is a powerful method against external disturbances and model uncertainties [18]. Therefore, the MPC strategy is capable of explicitly handling constraints and nonlinearities as well as optimizing the control performance [19]. Considering the advantages of MPC in constraint handling and anticipating the reference trajectory, it has been widely applied in EHSS. In this regard, Froehlich designed a constraint MPC for an injection molding machine driven by the servo pump [20]. Yuan proposed an MPC strategy for force tracking EHSS by grey-box identification of model parameters [21]. Heybroek designed an MPC for a hydraulic multi-chamber actuator to precisely control the force, while reducing the energy consumption [22]. Marusak proposed an MPC for a

single-rod hydraulic actuator with force feedback [23]. However, the complex pump-controlled EHSS with fast response and without overshoot has not been investigated. Moreover, full-state feedback was applied in all aforementioned MPC for EHSS, thereby increasing the investigation expenses.

Inspired by the tracking differentiator (TD) and nonlinear extended state observer (ESO), an MPC with lumped disturbance compensation was proposed in the present study. To avoid the overshoot problem in the fast response, the TD was used to implement the command planning of the fin servo system originating from the central control unit. Moreover, ESO was applied to take large uncertainties, heavy disturbances and high nonlinearities as the lumped disturbance [24]. Meanwhile, the lumped disturbance was compensated directly by minimizing the objective function. Since an accurate fin angle control only depends on the fin angle feedback sensor and the swashplate feedback sensor, the EHSS was implemented.

The present article is organized as follows: The model of pump-controlled EHSS was expressed in Section 2. Then the MPC control strategy, TD, ESO and the corresponding handling constraints were discussed in Section 3. In Section 4, the obtained results are analyzed. Finally, the main achievements and conclusions are summarized in Section 5.

2 MODEL OF THE FIN STABILIZER EHSS

2.1 Principle Description

Fig. 1 illustrates the schematic diagram of the servo system for the fin stabilizer, indicating that a closed hydraulic circuit consists of the variable pump and two hydraulic cylinders.

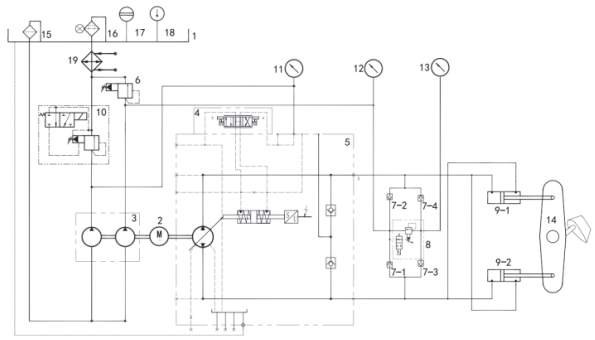

1. Oil tank, 2. Motor, 3. Gear pump, 4. Servo valve, 5. Variable pump, 6, 8, 10. Relief valve, 7. Check valve, 9. Hydraulic cylinder, 11, 12, 13. Pressure gauge, 14. Rocker arm, 15, 16. Filter, 17. Oil level sensor, 18. Oil temperature sensor, 19. Cooler

Figure 1 Schematic diagram of the fin servo system

The pump is driven by a motor and provides the required hydraulic power for hydraulic cylinders. The rotation direction and velocity of the fin are determined by the swashplate, which is controlled by an electro-hydraulic servo valve (SV). The hydraulic pressure on the high-pressure side of the closed-circuit is affected by the applied load on the rocker arm. Moreover, a pressure gauge is used to monitor the pressure. The first outlet of the double gear pump is employed to replenish oil to the low-pressure side of the closed-circuit through four check valves and an electromagnetic relief valve. It is worth noting that the hydraulic pressure in the replenishment circuit can be adjusted through the relief valve. A pressure gauge is installed in this regard to monitor the hydraulic pressure. The second outlet of the gear pump is used to control the angle of the swashplate through a SV. The pressure of the control circuit can be adjusted through the relief valve-, and a pressure gauge is installed to show the pressure.

2.2 Modeling the Swashplate System

The flow equation of the SV can be linearized as [25]:

$$Q_{sL} = K_{sq} x_{sv} - K_{sc} p_{sL} \tag{1}$$

where Q_{sL} is the flow rate, K_{sq} is the gain coefficient, x_{sv} denotes the spool displacement, K_{sc} is the pressure coefficient and p_{sL} is the pressure drop of the load.

Moreover, the equation of the cylinder flow in the displacement system can be expressed in the form below:

$$Q_{sL} = A_s \dot{y}_s + C_{stc} p_{sL} + V_{st} \dot{p}_{sL} / \left(4\beta_{se}\right) \tag{2}$$

where A_s and $\dot{y}_s$ are the effective area of the piston and the cylinder piston rod, respectively. Meanwhile, C_{stc} is the total leakage coefficient, V_{st} is the total volumes of two chambers and β_{se} denotes the bulk modulus of oil.

Neglecting the oil mass, the force balance equation between the cylinder piston and the external load can be expressed as follows:

$$A_s p_{sL} = m_s \ddot{y}_s + b_{sc} \dot{y}_s + K_{ss} y_s + F_s \tag{3}$$

where m_s is the equivalent load, b_{sc} and K_{ss} denote the viscous damping coefficient of the piston rod and the stiffness coefficient of load, respectively. Moreover, F_s is the unmodelled dynamic disturbance force. Since the swashplate is an inertia load K_{ss} and F_s can be ignored.

Under this assumption, the Laplace transform of the piston displacement can be expressed in the form below:

$$y_s = K_{sq} x_{sv} / (A_s A(s)) \tag{4}$$

where $K_{sce} = K_{sc} + C_{stc}$, s is the complex variable, $A(s) = \frac{m_s V_{st}}{4\beta_{se} A_s^2} s^3 + (\frac{m_s K_{sce}}{A_s^2} + \frac{b_{sc} V_{st}}{4\beta_{se} A_s^2}) s^2 + (1 + \frac{K_{sce} b_{sc}}{A_s^2}) s$.

Since the angle of the swashplate does not exceed ± 45 deg, the correlation between the swashplate angle and the displacement of the hydraulic cylinder can be expressed through the following expression:

$$\alpha_s = \arctan(y_s / R_s) \approx K_{sg} y_s \tag{5}$$

where R_s is the distance between the connection point and the supporting point of the swashplate mechanism in the pump, α_s is the swashplate angle and K_{sg} denotes the displacement gradient. Under this circumstance, the SV can be regarded as a second-order transfer function in the form below:

$$G_{sv}(s) = K_{sv}\omega_{sn}^2 / (s^2 + 2\xi_{sn}\omega_{sn}s + \omega_{sn}^2) \quad (6)$$

where K_{sv} and ω_{sn} are the gain and natural frequency of the SV, respectively. Meanwhile, ξ_{sn} is the non-dimensional damping ratio.

Since the conversion velocity of is breakneck, the amplifier of the servo drive can be expressed as:

$$K_{sa} = i_{sc} / u_{sc} \quad (7)$$

where K_{sa} is the component gain, i_{sc} is the input current and u_{sc} is the controller output of the swashplate system. When the feedback potentiometer has a much higher response frequency than that of the swashplate system, then the feedback component and its amplifier can be transformed to a proportional component with a unity gain.

Fig. 2 illustrates the block diagram of the swashplate system, where α_{sr} is the set value of the swashplate, $e_{sr} = \alpha_{sr} - \alpha_s$, and C_2 is the controller of the swashplate system. Other variables were previously defined in Eqs. (1) to (7).

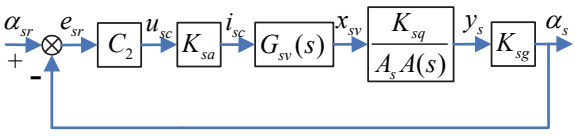

Figure 2 Block diagram of the swashplate control system

2.3 Modeling the Fin Angle Control System

The force couple structure of the rocker arm consists of two hydraulic cylinders, which can be equated with a symmetrical hydraulic cylinder. For the high-pressure chamber of the equivalent hydraulic cylinder, the flow continuity equation can be expressed in the form below [26]:

$$\begin{aligned} &n_p d_p - C_{pi}(p_{p1} - p_{pr}) - C_{pe}p_{p1} - C_{fe}p_{p1} = \\ &= A_f \dot{y}_f + V_{ft}\dot{p}_{p1} / \beta_{pe} \end{aligned} \quad (8)$$

where n_p and d_p are the speed and displacement of the pump, respectively. C_{pi} and C_{pe} are the internal and external leakage coefficients of the pump, respectively. C_{fe} is the external leakage coefficient of the equivalent cylinder. Moreover, p_{p1} and p_{pr} are the pressure of load and replenish oil, respectively. A_f and $\dot{y}_f$ are the effective area of the piston and the displacement of the piston rod, respectively. V_{ft} is the total volume of a chamber, β_{pe} denotes the effective bulk modulus of oil. The displacement of the variable pump can be described as follows [27]:

$$d_p = K_{p1}\alpha_s \quad (9)$$

where K_{p1} is the proportional coefficient between the displacement of the pump and the angle of the swashplate.

The force balance equation of the hydraulic cylinder can be expressed as [28]:

$$F_f = A_f p_{p1} = m_f \ddot{y}_f + b_{fc}\dot{y}_f + F_{fd} \quad (10)$$

where F_f is the force of the hydraulic cylinder, m_f and b_{fc} are the total mass and viscous damping coefficient of the piston rod and the load, respectively. F_{fd} is the external load force acting on the piston rod.

The replenished oil pressure is a small constant so that it can be ignored. Accordingly, the Laplace transformation can be rewritten in the form below:

$$n_p K_{p1}\alpha_s = A_f s y_f + (V_{ft}s / \beta_{pe} + C_{ft})p_{p1} \quad (11)$$

where $C_{tf} = C_{ip} + C_{ep} + C_{ef}$ is the total leakage coefficient of the system. Then the transfer function from the swashplate angle to the displacement of the cylinder rod y_f can be expressed as follows:

$$y_f = (A_f n_p K_{p1}\alpha_s - (V_{ft}s / \beta_{pe} + C_{ft})F_{fd}) / B(s) \quad (12)$$

where $B(s) = m_f V_{ft}s^3 / \beta_{pe} + (m_f C_{ft} + b_{fc}V_{ft} / \beta_{pe})s^2 + (A_f^2 + b_{fc}C_{ft})s$.

Similar to Eq. (5) and when the fin angle is less than 45 deg, the correlation between the fin angle and the displacement of the cylinder rod can be linearized in the form below:

$$y_f = K_{fa}\alpha_f \quad (13)$$

where α_f is the fin angle and K_{fa} is the proportional coefficient.

When the feedback potentiometer has a much higher response frequency than the hydraulic system, the feedback unit and its amplifier of the fin angle can be transformed to a proportional component with unit gain.

Fig. 3 illustrates the block diagram of the fin stabilizer electro-hydraulic servo system where α_{fr} is the input of the fin EHSS from the central control system of the fin stabilizer and C_1 is the controller of the fin angle control system $e_{fr} = \alpha_{fr} - \alpha_f$.

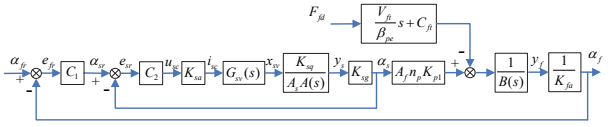

Figure 3 The block diagram of the fin EHSS

To make the fin angle α_f accurately follows the command α_{fr} from the central control unit of fin stabilizer, it is necessary that the force provided by the hydraulic cylinders to balance the external load force F_{fd} dynamically. The external load force can be expressed as:

$$F_{fd} = (M_{fs} + M_{ff} + M_{fu} + J_f(d^2\alpha_f)/dt^2)/l_{ar} \quad (14)$$

where M_{fs} is the moment of fin shaft cause by the hydrodynamic force on fin. M_{ff} presents the friction moment between the fin shaft and the hull. M_{fu} is used to describe the unbalanced moment induced from the gravity and buoyancy of fin. J_f is the total moment of inertia due to the rocker arm, fin shaft, and fin. l_{ar} denotes half the length of the rocker arm.

The detail expresses of moment M_{fs} can be found in references [29-31].

The fin shaft can be regarded as a cantilever beam with two bearing-shaft interaction. Thereforce, the friction moment M_{ff} can be approximately described as [32].

$$M_{ff} = -r_{f1}\mu_{f1}(\dot{\alpha}_f)F_{f1} - r_{f2}\mu_{f2}(\dot{\alpha}_f)F_{f2} \quad (15)$$

where r_{f1} and r_{f2} are the radius of the shaft segment at upper and lower bearing, respectively. μ_{f1} and μ_{f2}, respectively, denote the dynamic friction coefficien, which relate to the angluar speed of the fin $\dot{\alpha}_f$. F_{f1} and F_{f2} represent the contact force and each bearing, which can be calculated by the hydrodynamic force of the fin, the gravity of the shaft, and the gravity and buoyancy of the fin.

The unbalanced moment M_{fu} is expressed as:

$$M_{fu} = (F_{fg}l_{fg} - F_{fb}l_{fb})\cos(\alpha_f) \quad (16)$$

where F_{fg} and F_{fb} are the gravity and buoyancy of the fin respectively. l_{fg} and l_{fb} denote the distance from the center of gravity and buoyancy to the fin shaft, respectively.

It should be indicated that there exists a large nonlinearity and uncertainty in the parameters of the pump-control hydraulic system such as bulk modulus β_{se} and β_{pe}, flow gain of the SV K_{sq}, displacement coefficient of the pump K_{p1}, load pressure p_{p1} and external load force F_{fd}. Therefore, it is an enormous challenge to obtain precise model parameters.

3 CONTROLLER DESIGN FOR EHSS

Although the fin EHSS can be controlled through simple PID feedback, the MPC-based model can improve the control precision so that it can be applied in more systems. In the present study, it is intended to design an MPC for a servo system to meet the required performance when the fin stabilizer is used at zero speed. To this end, the fin angle subsystem model in the EHSS can be rewritten as follows [33, 34]:

$$\begin{aligned} \dot{x}_1 &= x_2 \\ \dot{x}_2 &= x_3 \\ \dot{x}_3 &= f_1(\cdot) + K_{fb}\alpha_s + d \end{aligned} \quad (17)$$

where $x_1 = \alpha_f$, $x_2 = \dot{\alpha}_f$, $x_3 = \ddot{\alpha}_f$, d denotes the lumped disturbance that includes nonlinearity and uncertainty of EHSS in $f_1(\cdot)$ and the external disturbance, $f_1(\cdot) = -(\beta_{pe}m_f C_{ft} + b_{fc}V_{ft})x_3/(V_{ft}m_f) - (A_f^2 + b_{fc}C_{ft})\beta_{pe}x_2/(V_{ft}m_f)$, $d = (V_{ft}\dot{F}_{fd} + \beta_{pe}C_{ft}F_{fd})/(V_{ft}m_f K_{fa})$ and $K_{fb} = (A_f n_p K_{p1}\beta_{pe})/(V_{ft}m_f K_{fa})$.

Based on Eq. (17), a state-space model can be expressed in the form below:

$$\begin{aligned} \dot{x} &= A_c x + B_c u + D_c d \\ y &= C_c x \end{aligned} \quad (18)$$

where $x = [x_1, x_2, x_3]^T$, $u = \alpha_s$, $A_c \in R^{n\times n}$ and $C_c \in R^{1\times n}$ are the state matrix and output matrix, respectively. Moreover, $B_c \in R^{n\times 1}$ and $D_c \in R^{n\times 1}$ are the input matrix and disturbance matrix, respectively. n denotes the initial orders of the system. It should be indicated that for the EHSS of the fin stabilizer, the lumped disturbance d is bounded and differentiable.

The MPC with a disturbance compensation should deal with the constrained system and reject the lumped disturbance by an online optimization. Generally, the optimization progress is performed by a digital processing unit. Therefore, it is necessary to establish an appropriate discretized model. This model can be obtained by a first-order Euler method as follows [35]:

$$\begin{aligned} x(k+1) &= A_d x(k) + B_d u(k) + D_d d(k) \\ y(k) &= C_d x(k) \end{aligned} \quad (19)$$

where k is the discrete step at a time kT_s and T_s is the sampling interval. In this regard, Jimoh applied the differential form of Eq. (19) to design the controller and deal with the fast-varying lumped disturbance d [36].

$$\begin{aligned} \bar{x}(k+1) &= \bar{A}\bar{x}(k) + \bar{B}\bar{u}(k) + \bar{D}\bar{d}(k) \\ y(k) &= \bar{C}\bar{x}(k) \end{aligned} \quad (20)$$

where $\bar{u}(k) = u(k) - u(k-1)$, and $\bar{d}(k) = d(k) - d(k-1)$ are the increment in the state, control, and the lumped disturbance, respectively. $\bar{x}(k) = \begin{bmatrix} x(k) - x(k-1) \\ y(k-1) \end{bmatrix} \in R^{n+1}$, Furthermore, $\bar{A} = \begin{bmatrix} A_d & 0 \\ C_d & I \end{bmatrix}, \bar{B} = \begin{bmatrix} B_{d1} \\ 0 \end{bmatrix}, \bar{C} = \begin{bmatrix} C_d & I \end{bmatrix}$, are the system matrices.

3.2 Angle Command Planning

To avoid the overshoot of the fin EHSS at zero speed, a transient angle command should be constructed that the servo system follows. In this regard, the fastest convergence function was employed to perform the command planning.

$u_h = \text{fhan}(z_1, z_2, r_0, h_0) =$

$$\begin{cases} d = r_0 h_0^2, a_0 = h_0 z_2, y = z_1 + a_0 \\ a_1 = \sqrt{d(d+8|y|)} \\ a_2 = a_0 + \text{sign}(y)(a_1 - d)/2 \\ s_y = (\text{sign}(y+d) - \text{sign}(y-d))/2 \\ a = (a_0 + y - a_2)s_y + a_2 \\ s_a = (\text{sign}(a+d) - \text{sign}(a-d))/2 \\ u_h = -r_0(a/d - \text{sign}(a))s_a - r_0 \text{sign}(a) \end{cases} \tag{21}$$

where z_1 and z_2 are input variables, r_0 and h_0 are control parameters. In Eq. (21), these parameters are set to $z_1(k) = \alpha^*_{fr}(k) - \alpha_{fr}(k)$, $z_2(k) = \omega^*_{fr}(k)$, $h_0 = T_s$, where T_s is the sampling interval, k is the discrete step at time kT_s, $\alpha^*_{fr}(k)$ and $\omega^*_{fr}(k)$ are the fin angle and angular rate command, respectively. Accordingly, the command planning can be expressed as follows:

$$\begin{cases} f_h = \text{fhan}(\alpha^*_{fr}(k) - \alpha_{fr}(k), \omega^*_{fr}(k), r_0, T_s) \\ \alpha^*_{fr}(k+1) = \alpha^*_{fr}(k) + T_s \omega^*_{fr}(k) \\ \omega^*_{fr}(k+1) = \omega^*_{fr}(k) + T_s f_h \end{cases} \tag{22}$$

Then Eq. (21) guarantees the fastest command that minimizes the error $\alpha_f(k) - \alpha_{fr}(k)$ without overshoot [37].

3.3 Controller Design

The fin angle control with a constrained swashplate angle and swashplate angular rate can be regarded as a predictive control problem. Accordingly, the control increment can be obtained by solving the following equation:

$$J(k) = \frac{1}{2}\sum_{m=0}^{Np-1}(\|E(k+m)\|_Q^2 + \|\bar{u}(k+m)\|_R^2 + \|\bar{v}(k+m)\|_P^2) + \\ + \frac{1}{2}\|E(k+Np)\|_S^2 \tag{23}$$

subjected to $\underset{m=0,\,N_p-1}{|u(k+m)|} \le u_{\max}$ and $|\bar{u}(k+m)| \le \bar{u}_{\max}$ conditions, where $\|z\|_Q^2 = z^T Q z$, and $m = 0, \ , N_p - 1$

$E(k) = \begin{bmatrix} \alpha_f(k) - \alpha^*_{fr}(k) \\ \omega_f(k) - \omega^*_{fr}(k) \end{bmatrix}$ denote the tracking error. Moreover, $\bar{v}$ is used to simulate the lumped disturbance increment. $u_{\max}$ and $\bar{u}_{\max}$ are the maximal angle and angle increment of the swashplate, respectively. N_p is the steps of the prediction horizon. The matrices Q and S are positive and semi-definite, while the matrices R and P are positive and definite. Meanwhile, the term $\|E(k+N_p)\|_S^2/2$ denotes the additional terminal cost item, which is used to ensure the controller stability. The matrix S is the unique solution of an algebraic Riccati equation $S = \bar{A}^T S \bar{A} + Q - \bar{A}^T S \bar{B}(R + \bar{B}^T S \bar{B})^{-1} \bar{B}^T S \bar{A}$ [38].

The main objective of optimizing the MPC is to seek the following control sequences by minimizing the cost function $J(k)$.

$$\eta = [\bar{u}_k^T, \bar{u}_{k+1}^T, \cdots, \bar{u}_{k+N_p-1}^T, \bar{v}_k^T, \bar{v}_{k+1}^T, \cdots, \bar{v}_{k+N_p-1}^T]^T \tag{24}$$

Then the solution can be transformed to the following quadratic program:

$$\eta^* = \arg\min_{\eta} \eta^T H \eta / 2 + \eta^T F \bar{x}_e(k) \tag{25}$$

subjected to $L\eta \le b$, where L and b are employed to limit the magnitude and rate of the swashplate. These parameters will be discussed in detail in the following subsection. The matrix F and Hessian matrix H are calculated online at all intervals. These matrices are defined as follows:

$$H = \begin{bmatrix} B_M^T Q_M B_M + R_M & (D_M^T Q_M B_M)^T \\ D_M^T Q_M B_M & D_M^T Q_M D_M + P_M \end{bmatrix},$$

$$F^T = \begin{bmatrix} A_M^T Q_M B_M & A_M^T Q_M D_M \\ -C_M B_M & -C_M D_M^T \end{bmatrix},$$

$$B_M = \begin{bmatrix} \bar{B} & 0 & \cdots & 0 \\ \bar{A}\bar{B} & \bar{B} & \cdots & 0 \\ \cdots & \cdots & \cdots & \cdots \\ \bar{A}^{N_p-1}\bar{B} & \bar{A}^{N_p-2}\bar{B} & & \bar{B} \end{bmatrix},$$

$$Q_M = \begin{bmatrix} \bar{C}^T Q \bar{C} & \cdots & 0 & 0 \\ \cdots & \cdots & \cdots & 0 \\ 0 & \cdots & \bar{C}^T Q \bar{C} & \cdots \\ 0 & \cdots & 0 & \bar{C}^T S \bar{C} \end{bmatrix},$$

$$R_M = \begin{bmatrix} R & \cdots & 0 \\ \cdots & \cdots & \cdots \\ 0 & \cdots & R \end{bmatrix},$$

$$D_M = \begin{bmatrix} \bar{D} & 0 & \cdots & 0 \\ \bar{A}\bar{D} & \bar{D} & \cdots & 0 \\ \cdots & \cdots & \cdots & \cdots \\ \bar{A}^{N_p-1}\bar{D} & \bar{A}^{N_p-2}\bar{D} & \cdots & \bar{D} \end{bmatrix}$$

$$P_M = \begin{bmatrix} P & \cdots & 0 \\ \cdots & \cdots & \cdots \\ 0 & \cdots & P \end{bmatrix},$$

$$A_M = \begin{bmatrix} \bar{A} \\ \bar{A}^2 \\ \cdots \\ \bar{A}^{N_p} \end{bmatrix}, \quad C_M = \begin{bmatrix} Q\bar{C} & \cdots & 0 & 0 \\ \cdots & \cdots & \cdots & 0 \\ 0 & \cdots & Q\bar{C} & 0 \\ 0 & \cdots & 0 & S\bar{C} \end{bmatrix}.$$

Furthermore, the state $\overline{x}_e(k)^T$ is defined as:

$$\overline{x}_e(k) = [\overline{x}(k), \cdots, \overline{x}(k), \alpha_{fr}^*(k), \cdots, \alpha_{fr}^*(k+N_p-1)]^T \tag{26}$$

To compensate for the lumped disturbance $\overline{d}(k)$, the optimal disturbance $\overline{v}*$ is obtained from the optimal η^*, which is calculated in all iterations. The increment of control command can be computed through the following expression:

$$\overline{u}_v(k) = \overline{u}^*(k) + \mu(k) \tag{27}$$

where $\mu(k)$ is employed to compensate the lumped disturbance $\overline{d}(k)$, while it is computed according to the optimal disturbance $\overline{v}^*(k)$. It should be indicated that the error $E(k)$ can be minimized when $\mu(k)$ satisfies the following condition:

$$\overline{B}\mu(k) = D(\overline{v}^*(k) - \hat{d}(k)) \tag{28}$$

where $\hat{d}(k)$ is an estimation for the lumped disturbance. Then $\mu(k)$ can be rewritten in the form below:

$$\mu(k) = (\overline{B}^T\overline{B})^{-1}\overline{B}^T\overline{D}(\overline{v}^*(k) - \hat{d}(k)) \tag{29}$$

3.4 Disturbance Estimation

In order to obtain $\hat{d}(k)$, an ESO is used to estimate $\overline{d}(k)$. Although it is simple to adjust the parameters in the linear ESO, the nonlinear ESO is more accurate and rapid considering fast-varying and stochastic disturbance [39-41]. In order to enhance the control effect, the following nonlinear ESO was employed to estimate the lumped disturbance and states $\hat{x}_2(k)$, $\hat{x}_3(k)$.

$$\begin{aligned}
&e = x_1(k) - \hat{x}_1(k)\\
&\hat{x}_1(k+1) = \hat{x}_1(k) + T_s(\hat{x}_2(k) + k_{o1}g_1(\theta^3 e))/\theta^2\\
&\hat{x}_2(k+1) = \hat{x}_2(k) + T_s(\hat{x}_3(k) + k_{o2}g_2(\theta^3 e))/\theta\\
&\hat{x}_3(k+1) = \hat{x}_3(k) + T_s(\hat{d}(k) + f_1(\cdot) + k_{o3}g_3(\theta^3 e) + K_{fb}u(k))\\
&\hat{d}(k+1) = \hat{d}(k) + T_s(\theta k_{o4}g_4(\theta^3 e))
\end{aligned} \tag{30}$$

where θ is the observer gain. Moreover, the coefficient k_{o1}, k_{o2}, k_{o3} and k_{o4} are selected to ensure that the following matrix is Hurwitz

$$M_K = \begin{bmatrix} -k_{o1} & 1 & 0 & 0 \\ -k_{o2} & 0 & 1 & 0 \\ -k_{o3} & 0 & 0 & 1 \\ -k_{o4} & 0 & 0 & 0 \end{bmatrix} \tag{31}$$

The nonlinear function g_i is represented as:

$$g_i(e) = \mathrm{fal}(e, \alpha_i, \lambda) = \begin{cases} e/(\lambda^{1-\alpha_i}), & |e| \le \lambda \\ |e|^{\alpha_i}\ \mathrm{sign}(e), & |e| > \lambda \end{cases} \tag{32}$$

where $\alpha_1 = \gamma$, $\alpha_2 = 2\gamma - 1$, $\alpha_3 = 3\gamma - 2$, and $\alpha_4 = 4\gamma - 3$, $\gamma \in (3/4, 1)$. When the disturbance $d(k)$ and states $x_2(k)$, $x_3(k)$ are estimated, the differential signal $\hat{d}(k)$ can be obtained. Therefore, the compensation item $\mu(k)$ of disturbance is computed by Eq. (29). The optimal control variable is used to control the swashplate in all time intervals as follows:

$$u^*(k) = u^*(k-1) + \overline{u}^*(k) + \mu(k) \tag{33}$$

3.5 Constraint Handling

The control variable in Eq. (20) is the actual angle of the swashplate α_s, while the control signal generated by Eq. (33) is the angle command of the swashplate α_{sr}. In order to ensure that α_s can track the variations of α_{sr} in time, it is necessary to limit the magnitude and rate of $u^*(k)$. In this regard, the limit of the swashplate angle can be mathematically expressed as:

$$\alpha_{sL} \le u^*(k) = \alpha_s(k) \le \alpha_{sU} \tag{34}$$

where α_{sL} and α_{sU} are the lower and upper magnitude limits of the swashplate angle, respectively. Moreover, the rate limit of the swashplate angle can be expressed as the increment limit in the form below:

$$\overline{\alpha}_{sL} \le \overline{u}^*(k) \le \overline{\alpha}_{sU} \tag{35}$$

where $\overline{\alpha}_{sL}$ and $\overline{\alpha}_{sU}$ are the lower and upper incremental limits of the swashplate angle, respectively. It is worth noting that the increment limit is $\overline{u}^*(k)$ rather than $\overline{u}(k)$ for the introduction of the disturbance compensation $\mu(k)$. Eq. (29) can be simplified as the following:

$$\mu(k) = \Phi(\overline{v}^*(k) - \hat{d}(k)) \tag{36}$$

where $\Phi = (\overline{B}^T\overline{B})^{-1}\overline{B}^T\overline{D}$. Then the magnitude limit is represented by the following inequality:

$$\begin{bmatrix} L_1 & L_2 \\ -L_1 & -L_2 \end{bmatrix}\eta \le \begin{bmatrix} U_{sU} \\ -U_{sL} \end{bmatrix} - \begin{bmatrix} I_s \\ -I_s \end{bmatrix}u(k-1) + \begin{bmatrix} I_s \\ -I_s \end{bmatrix}\Phi\hat{d}(k) \tag{37}$$

where

$$L_1 = \begin{bmatrix} I & 0 & \cdots & 0 \\ I & I & \cdots & 0 \\ \cdots & \cdots & \cdots & \cdots \\ I & I & \cdots & I \end{bmatrix},\ L_2 = \begin{bmatrix} \Phi & \Phi & \cdots & 0 \\ \Phi & \Phi & \cdots & 0 \\ \cdots & \cdots & \cdots & \cdots \\ \Phi & \Phi & \cdots & \Phi \end{bmatrix},$$

$$I_s=\begin{bmatrix} I \\ I \\ \cdots \\ I \end{bmatrix}, U_{sU}=\begin{bmatrix} \alpha_{sU} \\ \alpha_{sU} \\ \cdots \\ \alpha_{sU} \end{bmatrix}, U_{sL}=\begin{bmatrix} \alpha_{sL} \\ \alpha_{sL} \\ \cdots \\ \alpha_{sL} \end{bmatrix}.$$

Similarly, the increment limit can be represented through the following inequality:

$$\begin{bmatrix} L_3 & L_4 \\ -L_3 & -L_4 \end{bmatrix}\begin{bmatrix} \bar{\bar{u}} \\ \bar{\bar{v}} \end{bmatrix} \le \begin{bmatrix} \bar{U}_{sU} \\ -\bar{U}_{sL} \end{bmatrix} + \begin{bmatrix} I_s \\ -I_s \end{bmatrix} \Phi \hat{d}(k) \tag{38}$$

where $\bar{\bar{u}}$ and $\bar{\bar{v}}$ are the increments of $\bar{u}$ and $\bar{v}$, respectively.

$$L_3=\begin{bmatrix} I & 0 & \cdots & 0 \\ 0 & I & \cdots & 0 \\ \cdots & \cdots & \cdots & \cdots \\ 0 & 0 & \cdots & I \end{bmatrix}, \quad L_4=\begin{bmatrix} \Phi & 0 & \cdots & 0 \\ 0 & \Phi & \cdots & 0 \\ \cdots & \cdots & \cdots & \cdots \\ 0 & 0 & \cdots & \Phi \end{bmatrix},$$

$$I_s=\begin{bmatrix} I \\ I \\ \cdots \\ I \end{bmatrix}, \bar{U}_{sU}=\begin{bmatrix} \bar{\alpha}_{sU} \\ \bar{\alpha}_{sU} \\ \cdots \\ \bar{\alpha}_{sU} \end{bmatrix}, U_{sL}=\begin{bmatrix} \bar{\alpha}_{sL} \\ \bar{\alpha}_{sL} \\ \cdots \\ \bar{\alpha}_{sL} \end{bmatrix}.$$

3.6 Controller Design of the Swashplate

In this section, the controller of the swashplate is used to adjust the angle of the swashplate by controlling the SV. Moreover, the swashplate angle follows the output of the MPC-based fin angle controller.

Due to relatively small variations of the working load and working pressure in the swashplate system, a PD controller is used to generate the control signal of the voltage current transformation circuit according to error e_{sr}.

$$\begin{aligned} &u_{sc}(k)=K_{sp}e_{sr}(k)+\beta_{cs}u_{sd}(k-1)+ \\ &K_{sd}(1-\beta_{cs})(e_{sr}(k)-e_{sr}(k-1))/T_s \end{aligned} \tag{39}$$

where K_{sp} and K_{sd} are the proportional and differential coefficients in the swashplate controller, respectively. Moreover, T_s is the sampling interval. The coefficient β_{cs} is introduced to implement the incomplete differentiation algorithm, which can decrease the influence of the high-frequency noise in the ship engine room. Furthermore, $\beta_{cs}<1, 1-\beta_{cs}<1$.

3.7 Stability and Recursive Feasibility Analysis

The object function Eq. (23) can be transformed to a new function

$$\begin{aligned} &J(k)=\frac{1}{2}\sum_{m=0}^{Np-1}\left(\left\|E(k+m)\right\|_Q^2+\left\|\bar{u}_n(k+m)\right\|_{Rn}^2+\right. \\ &\left.+\frac{1}{2}\left\|E(k+N_p)\right\|_S^2\right. \end{aligned} \tag{40}$$

while the new maxtirx R_n was defined as

$$R_n=\begin{bmatrix} R & 0 \\ 0 & P \end{bmatrix}. \tag{41}$$

The optimal solution of Eq. (40) can be obtained by solving the standard MPC problem. Therefore, the additional deg of freedom in Eq. (23) is only for the convenience of handling disturbances, which can be degenerated to a standard object function of MPC. The stability and recursive feasibility can be ensured by the terminal constraint terms in standard MPC.

4 SIMULATION AND EXPERIMENT RESULTS

4.1 Simulation and Experiment Equipment

Fig. 4 shows that the pump-controlled EHSS for the fin stabilizer was used to evaluate the tracking performance of the proposed MPC control strategy. The fin EHSS consists of the hydraulic power unit (HPU) and the mechanical unit.

It is worth noting that the oil tank, motor, variable pump, cooler and local control unit constitute the HPU. The swashplate sensor and SV are mounted on the variable pump. The local control unit is employed to implement the operation and control of the EHSS and receive the operation instructions from the central control unit that is located in the centralized control room. A set of the programmable logic controller (PLC, the main control unit is the Wago 750-8203) in the local control unit is used to implement the MPC and the PD controller for the swashplate control.

The fin angle sensor, rocker arm, and two hydraulic cylinders together constitute the mechanical unit, which is connected to the HPU through two oil pipelines.

The loading simulation device is utilized to imitate the force of the seawater that is applied to the fin when the fin stabilizer operates. The loading simulation device is another hydraulic system that provides the loading moment on the fin shaft by two hydraulic cylinders and a rocker arm. The control system in the loading simulation device calculates the loading force according to the shipping speed, fin angle, and angular rate of the fin. Tab. 1 presents the main parameters of the tested EHSS.

4.2 Simulation Results

The simulations were implemented for the proposed MPC control strategy and a PID controller with anti-integral saturation. The PID controller is widely used in the EHSS of the conventional fin stabilizer with the following structure:

$$\begin{aligned} &u(k)=u_p(k)+u_i(k)+u_d(k)=K_{fp}e_{fr}(k)+K_{fi}esum+ \\ &K_{fd}(1-\beta_{cf})(e_{fr}(k)-e_{fr}(k-1))/T_s+\beta_{cf}u_d(k-1) \end{aligned} \tag{42}$$

where $esum=\begin{cases} i_l\,\mathrm{sgn}(\sum_{j=0}^{k}e_{fr}(j)T_s), & \sum_{j=0}^{k}e_{fr}(j)T_s > i_l \\ \sum_{j=0}^{k}e_{fr}(j)T_s, & |\sum_{j=0}^{k}e_{fr}(j)T_s| \le i_l \end{cases}$, i_l is the saturation limit of the integral action.

The step responses with a 40.0 deg fin angle were simulated first to verify the rapidity and overshoot of the controllers.

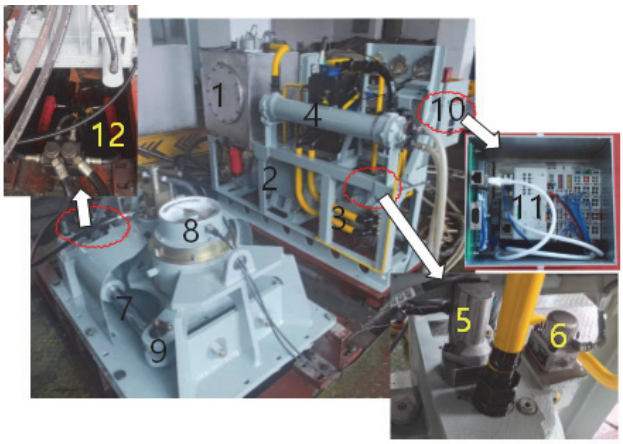

1. Oil tank, 2. Motor, 3. Variable pump, 4. Cooler, 5. Swashplate sensor, 6. Servo valve, 7. Hydraulic cylinder, 8. Fin angle sensor, 9. Rocker arm, 10. Local control unit, 11. PLC, 12. Loading simulation device

Figure 4 The tested EHSS of the fin

Table 1 Main parameters of the fin EHSS

Item	Value	Item	Value
Motor power	18.5 kw	Motor rated speed	1460.0 Rpm
Pump rated speed	3100.0 rpm	Pump displacement	130.0 ml/r
Rated flow of servo valve	30.0 L/min	Maximum angle of the swashplate	30 deg
Maximum pressure of fin angle system	14.0 MPa	Work pressure of swashplate system	7.0 MPa
Piston diameter of hydraulic cylinder	90.0 mm	Piston rod diameter of hydraulic cylinder	63.0 mm
Maximum fin angle	43.0 deg	Mechanical limit of fin angle	±45.0 deg
Cylinder stroke	425.0 mm	Maximum angular rate	55.0 deg/s

Fig. 5 describes the performance of the MPC and two PID controllers. The settling time is about 1.08s without overshoot when the PID1 ($K_{fp} = 0.5409$, $K_{fi} = 1.7892$, $K_{fd} = 0.00228$) controller is used. The settling time is about 0.72s with 3.26% overshoot when the PID2 controller is used ($K_{fp} = 0.708$, $K_{fi} = 1.2097$, $K_{fd} = 0.00345$). Moreover, the settling time is about 0.70s without overshoot when the MPC is employed. The proposed MPC has the better rapidity without overshoot. However, it is difficult to balance the rapidity and stability for the PID controller, the overshoot will occur with the increase of rapidity.

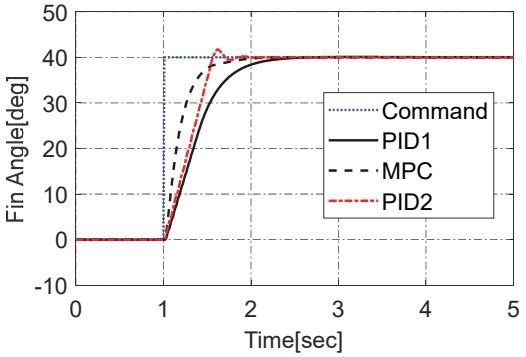

Figure 5 The comparison of simulation with different controllers

To imitate the fin motion on conventional mode, the tracking performance of a regular wave and an irregular wave was further simulated. Fig. 6 illustrates the simultaion results when these controllers followed the sine command with the T_ϕ period and 26.0 deg amplitude to mimic the ship voyage on the regular ocean waves with 18.0 kn speed. Where T_ϕ = 9.0 is the resonat period of the ship. The amplitude is 25.67 deg with 11.60 deg of phase lag when the PID1 controller is used. The amplitude is 26.02 deg with 1.20 deg of phase lag when the PID2 controller is used. However, the amplitude is 25.99 deg with 0.70 deg of phase lag when the MPC is used. Fig. 7 illustrates the simultaion results when these controllers followed the command of the irregular wave. The simulation results on regular and irregular show that the PID controller and the MPC can meet the performace requirments when the fin stabilizer works on the conventional mode. But the MPC has the better performance of the smaller amplitude error and phase lag.

To imitate the fin motion on zero-speed mode, it is observed that the fin flaps rapidly between –43.0 deg and +43.0 deg. When the flapping is regarded as a step response from –43.0 deg to +43.0 deg, the settling time is about 1.30 s with overshoot and oscillation when the PID1 controller is used. The settling time is about 1.21 s with overshoot and oscillation when the PID2 controller is employed, but the maximum fin angle is over 47.31 deg. It cannot be realized in the actual mechanism for the maximum mechanical limit angle is 45.0 deg. Moreover, the settling time is about 1.20 s without overshoot when the proposed MPC controller is utilized. Only the MPC can meet the performace requirments without overshoot when the fin stabilizer works on the zero-speed mode.

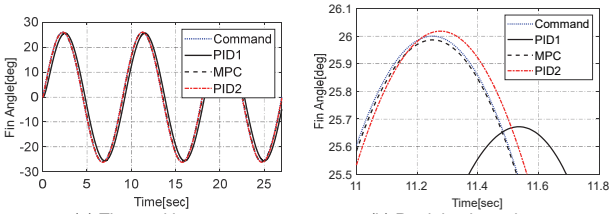

(a) The tracking curves (b) Partial enlarged curves

Figure 6 The tracking performance of regular wave

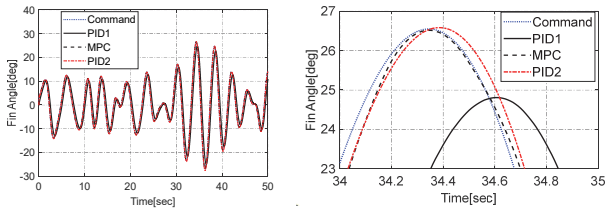

(a) The tracking curves (b) Partial enlarged curves

Figure 7 The tracking performance of irregular wave

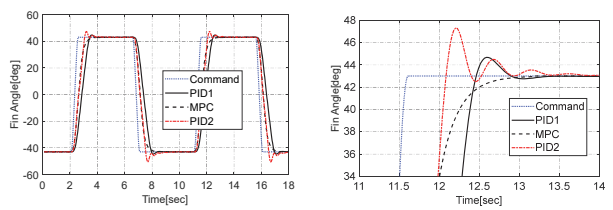

(a) Instruction tracking (b) Partial enlarged tracking

Figure 8 The comparison of the tracking performance with different controllers

4.3 Experiment Results

The experiments were implemented to further verify the tracking performance with different controllers. The step responses with a 40.0 deg fin angle were initially implemented to verify the rapidity and overshoot. Fig. 9 illustrates the tracking performance of the three controllers. The settling time is about 1.13 s without overshoot when the PID1 controller is used. Moreover, the settling time is about 0.92 s when the PID2 controller is used. It should be indicated that overshoot appears and the static error decreases while PID2 controlller is used. The settling time is about 0.79 s without overshoot when the proposed MPC is used. Moreover, there is almost no static error.

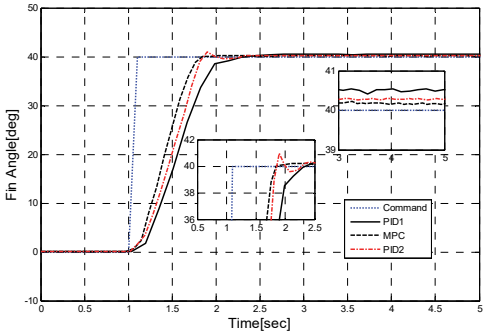

Figure 9 The comparison of step response with a different controller

Fig. 10 shows the tracking performance when the fin stabilizer operates at zero speed. When the flapping is regarded as a step response from –43.0 deg to +43.0 deg, the settling time is about 1.37 s with overshoot and oscillation when the PID1 controller is used. Moreover, the settling time is about 1.26 s without overshoot when the proposed MPC controller is utilized. The rocker arm will strike the mechanical limiter in the mechanical unit when the PID2 controller is employed. Therefore, the experiment cannot be implemented.

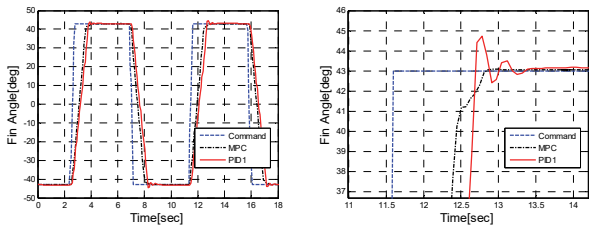

(a) Instruction tracking (b) Partial enlarged tracking

Figure 10 The comparison of the tracking performance with different controllers

The difficulty of the controller is to satisfy the use of the EHSS at zero-speed mode. Tab. 2 describes the simulation and experiment results of different controllers. It can be concluded from the simulation and experiments results that the MPC has the smallest settting times without overshoot for the step response for –43.0 to 43.0 deg. The simulation results are in good agreement with the experimental results

There is no overshoot when the PID1 controller is used in the step test from 0 to 40.0 deg. However, the overshoot occurs when it operates at zero-speed mode. The partially enlarged detail shows that oscillation appears, which not only enhances the noise in HPU and mechanical unit but also increases the mechanical wear and shock. Compared with the MPC, the increased adjustment time and overshoot when the PID1 controller is employed will reduce the stabilization force that is generated by the fin and decrease the damping effectiveness of the fin stabilizer at zero speed.

Table 2 The comparison of the tracking performance with different controllers

Controller	Instruction	Condition	Setting time / s	Overshoot / %
PID1	Step (0 to 40.0°)	Simulation	1.08	0.00
		Experiment	1.13	0.00
	Step (–43.0 to 43.0°)	Simulation	1.30	1.95
		Experiment	1.37	1.98
PID2	Step (0 to 40.0°)	Simulation	0.72	3.26
		Experiment	0.92	2.81
	Step (–43.0 to 43.0°)	Simulation	1.21	5.01
MPC	Step (0 to 40.0°)	Simulation	0.70	0.00
		Experiment	0.79	0.00
	Step (–43.0 to 43.0°)	Simulation	1.20	0.00
		Experiment	1.26	0.00

5 CONCLUSIONS

In the present study, the model of a pump-controlled electro-hydraulic servo system for the fin stabilizer was constructed. In order to deal with the constraints of swashplate angle and angular rate, a constrained MPC for incremental EHSS model was proposed. Moreover, a nonlinear extended states observer was employed to estimate the angular rate, angular accelerator of fin, the uncertainty, nonlinearity in the EHSS model, and the external disturbance. It should be indicated that the tracking performance of the proposed MPC control strategy was verified by the simulation and experiment of a fin EHSS that will be installed on a ship. The simulation and experimental results show that the proposed MPC controller meets the requirements listed in the Section 1 when the fin stabilizer is used at zero speed.

It is worth noting that the electric current of the motor variates with the alternate movement of the fin between flapping and stopping. This will disturb the voltage and frequency of the grid, while the ship generator cannot provide enough power. Therefore, decreasing the current variance by improving both the hydraulic system and control strategy without deteriorating the tracking performance will be investigated in future works.

Acknowledgments

This work was supported by the National Natural Science Foundation of China [grant numbers 50879012 and 50575048].

6 REFERENCES

[1] Shang, Y. X., Li, R. J., Wu, S. et al. (2022). A Research of High-Precision Pressure Regulation Algorithm Based on ON/OFF Valves for Aircraft Braking System. *IEEE Transactions on Industrial*, *69*(8), 7797-7806. https://doi.org/10.1109/TIE.2021.3108705

[2] Wei, S., Liu, X. Y., & Su, X. Y. (2021). High-Precision Position Tracking Control of Electro-hydraulic Servo Systems Based on an Improved Structure and Desired Compensation. *International Journal of Control, Automation and Systems*, *19*(11), 3622-3630.

https://doi.org/10.1007/s12555-020-0705-1
[3] Hyon, S. H., Suewaka, D., Torii, Y., & Oku, N. (2017). Design and Experimental Evaluation of a Fast Torque-Controlled Hydraulic Humanoid Robot. *IEEE-ASME Transactions on Mechatronics*, *22*(2), 623-634. https://doi.org/10.1109/TMECH.2016.2628870
[4] Koivumaki, J., Zhu, W. H., & Mattila, J. (2019). Energy-efficient and high-precision control of hydraulic robots. *Control Engineering Practice*, *85*, 176-193. https://doi.org/10.1016/j.conengprac.2018.12.013
[5] Zhu, R., Yang, Q. J., Liu, Y. D. et al. (2022). Sliding Mode Robust Control of Hydraulic Drive Unit of Hydraulic Quadruped Robot. *International Journal of Control, Automation and System*s, *20*(4), 1336-1350. https://doi.org/10.1007/s12555-021-0235-5
[6] Li, J. Y., Wang, Y. W., & Wang, X. J. (2014). Research on electro-hydraulic force servo system based on neural network and fuzzy intelligent control strategy. *Journal of Computational and Theoretical Nanoscience*, *11*(4), 1205-1210. https://doi.org/10.1166/jctn.2014.3484
[7] Jiao, Z. X., Zhang, H., Shang, Y. X. et al. (2020). A power-by-wire aircraft brake system based on high-speed on-off valves. *Aerospace Science and Technology*, *106*, 10177. https://doi.org/10.1016/j.ast.2020.106177
[8] Martin, I. A. & Irani, R. A. (2021). Dynamic modeling and self-tuning anti-sway control of a seven degree of freedom shipboard knuckle boom crane. *Mechanical Systems and Signal Processing*, *153*, 107441. https://doi.org/10.1016/j.ymssp.2020.107441
[9] Thomas, A. T., Parameshwaran, R., Sathiyavathi, S., & Starbino, A. V. (2019). Improved Position Tracking Performance of Electro Hydraulic Actuator Using PID and Sliding Mode Controller. *IETE Journal of Research*. https://doi.org/10.1080/03772063.2019.1664341
[10] Shen, W., Wang, J., Huang, H., & He, J. (2019). Fuzzy sliding mode control with state estimation for velocity control system of hydraulic cylinder using a new hydraulic transformer. *European Journal of Control*, *48*, 104-114. https://doi.org/10.1016/j.ejcon.2018.11.005
[11] Guo, Q., Zuo, Z. Y., & Ding, Z. T. (2020). Parametric adaptive control of single-rod electrohydraulic system with block-strict-feedback model. *Automatica*, *113*. https://doi.org/10.1016/j.automatica.2020.108807
[12] Chaudhuri, S., Saha, R., & Chatterjee, A. (2020). Adaptive neural-bias-sliding mode control of rugged electrohydraulic system motion by recurrent Hermite neural network. *Control Engineering Practice*, 104588. https://doi.org/10.1016/j.conengprac.2020.104588
[13] Peng, X. J., Chen, G. Z., & Tang, Y. J. (2020). Trajectory optimization of an electro-hydraulic robot. *Journal of Mechanical Science and Technology*, *34*(10), 4281-4294. https://doi.org/10.1007/s12206-020-0919-4
[14] Lee, W., Yoo, S., & Nam, S. (2020). Passivity-Based Robust Compliance Control of Electro-Hydraulic Robot Manipulators With Joint Angle Limit. *IEEE Robotics and Automation Letters*, *5*(2), 3190-3197. https://doi.org/10.1109/LRA.2020.2975724
[15] Sun, M. X., Luan, T. T., & Liang, L. H. (2018). RBF neural network compensation-based adaptive control for lift-feedback system of ship fin stabilizers to improve anti-rolling effect. *Ocean Engineering*, *163*, 307-321. https://doi.org/10.1016/j.oceaneng.2018.06.011
[16] Lyu, L. T., Chen, Z., & Yao, B. (2021). Advanced Valves and Pump Coordinated Hydraulic Control Design to Simultaneously Achieve High Accuracy and High Efficiency. *IEEE Transactions on Control Systems Technology*, *29*(1), 236-248. https://doi.org/10.1109/TCST.2020.2974180
[17] Song, J. G., Zhao, P., Liang, L. H., & Ji, M. (2020). Force modeling of zero/low-velocity fin stabilizer and hydrofoil profile optimization. *Ocean Engineering*, *213*. https://doi.org/10.1016/j.oceaneng.2020.107635
[18] Liao-McPherson, D., Nicotra, M. M., & Kolmanovsky, I. (2020). Time-distributed optimization for real-time model predictive control: Stability, robustness, and constraint satisfaction. *Automatica*, *117*, 180973. https://doi.org/10.1016/j.automatica.2020.108973
[19] Wei, H. L., Sun, Q. J.,Chen, C., & Shi, Y. (2021). Robust distributed model predictive platooning control for heterogeneous autonomous surface vehicles. *Control Engineering Practice*, *107*, 104655. https://doi.org/10.1016/j.conengprac.2020.104655
[20] Froehlich, C., Kemmetmueller, W., & Kugi, A. (2020). Model-Predictive Control of Servo-Pump Driven Injection Molding Machines. *IEEE Transactions on Control Systems Technology*, *8*(5), 1665-1680. https://doi.org/10.1109/TCST.2019.2918993
[21] Yuan, H. B.,Na, H. C., & Kim, Y. B. (2018). Robust MPC-PIC force control for an electro-hydraulic servo system with pure compressive elastic load. *Control Engineering Practice*, *79*, 170-184. https://doi.org/10.1016/j.conengprac.2018.07.009
[22] Heybroek, K. & Sjoberg, J. (2018). Model Predictive Control of a Hydraulic Multichamber Actuator: A Feasibility Study. *IEEE-ASME Transactions on Mechatronics*, *23*(3), 1393-1403. https://doi.org/10.1109/TMECH.2018.2823695
[23] Marusak, P. M. & Kuntanapreeda, S. (2011). Constrained model predictive force control of an electrohydraulic actuator. *Control Engineering Practice*, *19*(1), 62-73. https://doi.org/10.1016/j.conengprac.2010.09.002
[24] Zhang, D. Y., Liu, S. Y., Chen, Y., & Gu, C. C. (2022). Neural Direct Adaptive Active Disturbance Rejection Controller for Electro-hydraulic Servo System. *International Journal of Control, Automation and Systems*, *20*(7), 2402-2412. https://doi.org/10.1007/s12555-020-0954-z
[25] Fan, Y., Shao, J., Sun, G., &Shao, X. (2020). Proportional-Integral-Derivative Controller Design Using an Advanced Levy-Flight Salp Swarm Algorithm for Hydraulic Systems. *Energies*, *13*(2), 459. https://doi.org/10.3390/en13020459
[26] Yang, G. &Yao, J. (2020). High-precision motion servo control of double-rod electro-hydraulic actuators with exact tracking performance. *Isa Transactions*, *103*, 266-279. https://doi.org/10.1016/j.isatra.2020.03.029
[27] Guo, K. & Wei, J. (2013). Adaptive robust control of variable displacement pumps. *2013 American Control Conference*, 1112-1117.
[28] Wang, L., Zhao, D., Liu, F. et al. (2020). Active Disturbance Rejection Position Synchronous Control of Dual-Hydraulic Actuators with Unknown Dead-Zones. *Sensors*, *20*(21), 1-23. https://doi.org/10.3390/s20216124
[29] Wang, F., Jin, H. Z., & Qi, Z. G. (2009). Modeling for active fin stabilizers at zero speed. *Ocean Engineering*, *36*, 1425-1437. https://doi.org/10.1016/j.oceaneng.2009.07.013
[30] Piana, G. & Carpinteri, A. (2021). Long-span Suspension Bridge Flutter Analysis with Drag Force Effects. *Journal of Applied and Computational Mechanics*, *7*, 1077-1089.
[31] Song, J. G., Liang, L. H., Zhang, S. T., & Wang, J. M. (2020). Design and experimental investigation of a ga-based control strategy for a low-speed fin stabilizer. *Ocean Engineering*, *218*(1). https://doi.org/10.1016/j.oceaneng.2020.108234
[32] Huang, Q. W., Liu, H. G., & Ding, Z. (2019). Dynamical response of the shaft-bearing system of marine propeller shaft with velocity-dependent friction. *Ocean Engineering*, *189*(6). https://doi.org/10.1016/j.oceaneng.2019.106399
[33] Su, S. J., Zhu, Y. Y., & Li, C. J. (2020). Dual-valve parallel prediction control for an electro-hydraulic servo system. *Science Progress*, *103*(1), 1-21. https://doi.org/10.1177/0036850419875662
[34] Suh, S. & Kim, W. (2020). Nonlinear Position Control Using Differential Flatness Concept with Load Torque Observer for Electro Hydraulic Actuators with Sinusoidal Load Torque. *Mathematics*, *8*(9), 1484. https://doi.org/10.3390/math8091484

[35] Gu, W., Yao, J., Yao, Z., & Zheng, J. (2019). Output feedback model predictive control of hydraulic systems with disturbances compensation. *Isa Transactions*, *88*, 216-224. https://doi.org/10.1016/j.isatra.2018.12.007
[36] Jimoh, I. A., Kucukdemiral, I. B., Bevan, G., & Orukpe, P. E. (2020). Offset-free Model Predictive Control: A Study of Different Formulations with Further Results. *28th Mediterranean Conference on Control and Automation*, 671-676. https://doi.org/10.1109/MED48518.2020.9183056
[37] Han, J. Q. (2009). From PID to active disturbance rejection control. *IEEE Transactions on Industrial Electronics*, *56*(3), 900-906. https://doi.org/10.1109/TIE.2008.2011621
[38] Rawlings, J. B. & Mayne, D. Q. (2015). Model predictive control: theory and design. *Nob Hill Publishing, Madison*.
[39] Wu, Z. H. & Guo, B. Z. (2020). Active disturbance rejection control to MIMO nonlinear systems with stochastic uncertainties: approximate decoupling and output-feedback stabilization. *International Journal of Control*, *93*(6), 1408-1427. https://doi.org/10.1080/00207179.2018.1508854
[40] Stankovic, M. R., Madonski, R., Shao, S., & Mikluc, D. (2020). On dealing with harmonic uncertainties in the class of active disturbance rejection controllers. *International Journal of Control*. https://doi.org/10.1080/00207179.2020.1736639
[41] Yuan, Y., Yu, Y., Wang, Z. D., & Guo, L. (2019). A Sampled-Data Approach to Nonlinear ESO-Based Active Disturbance Rejection Control for Pneumatic Muscle Actuator Systems with Actuator Saturations. *IEEE Transactions on Industrial Electronics*, *66*(6), 4608-4617. https://doi.org/10.1109/TIE.2018.2864711

Contact information:

Jiguang SONG
College of Intelligent Systems Science and Engineering,
Harbin Engineering University,
Harbin Heilongjiang, 150001, China

Yanxin LIU
College of Intelligent Systems Science and Engineering,
Harbin Engineering University,
Harbin Heilongjiang, 150001, China

Jingfu WANG
(Corresponding author)
College of Intelligent Systems Science and Engineering,
Harbin Engineering University,
Harbin Heilongjiang, 150001, China
Email: Jingfuwang_hrbeu@163.com

Lihua LIANG
College of Intelligent Systems Science and Engineering,
Harbin Engineering University,
Harbin Heilongjiang, 150001, China

Nomenclature

A_c, B_c, C_c, D_c matrices of continuous system

A_d, B_d, C_d, D_d matrices of the discretized system

$\overline{A}, \overline{B}, \overline{C}, \overline{D}$ matrices of increment system

A_f effective piston area in the fin angle system, m^2

A_s effective piston area in the swashplate system, m^2

b_{fc} viscous damping coefficient in the fin angle system, N/(m/s)

b_{sc} viscous damping coefficient in the swashplate system, N/(m/s)

C_{fe} external leakage coefficient of the hydraulic cylinder, m^3/s/pa

C_{pi} internal leakage coefficient of the pump, m^3/s/Pa

C_{pe} external leakage coefficient of the pump, m^3/s/Pa

C_{stc} total leakage coefficient in the swashplate system, m^3/s/Pa

C_{tf} total leakage coefficient in the fin angle system, m^3/s/Pa

d lumped disturbance

d_p displacement of the variable pump, m^3/rad

n_p rotating speed of the variable pump, rad/s

N_p prediction horizon

p_{p1} load pressure, N/m^2

p_{pr} replenish oil pressure, N/m^2

p_{sL} pressure drop of the load, N/m^2

P, Q, R, S weight matrices

Q_{sL} load flow rate, m^3/s

R_s distance between the connection point and the supporting point of the swashplate, m

T_s sampling interval, s

u control variable in the fin angle system

$u_{\max}$ maximum of swashplate angle, rad

u_{sc} controller output in the swashplate system

u^* optimal control variable

$\overline{u}$ increment of the control variable

$\overline{u}_{\max}$ maximum increment of the swashplate angle

$\overline{u}_v$ increment of the control

$\overline{\overline{u}}, \overline{\overline{v}}$ increment of $\overline{u}, \overline{v}$

$\overline{v}$ simulated disturbance increment

$\overline{v}^*$ optimal disturbance increment

V_{ft} total volume in fin angle system, m^3

$\overline{d}$ increment of the lumped disturbance

$\hat{d}$ estimation of $\overline{d}$

e_{sr} tracking error of the swashplate angle, rad

e_{fr} tracking error of the fin angle, rad

F_f force provided by the hydraulic cylinder, N

F_{fd} external load force, N

F_s unmodelled disturbance force in the swashplate system, N

i_{sc} input current to the servo value, A

k discrete step

k_{oi} observer gain

K_{fa} proportional coefficient in the fin angle system, m/rad

K_{fd} differential coefficients in the fin angle controller

K_{fi} integral coefficient in the fin angle controller

K_{p1} proportional coefficient, m^3/rad/rad

K_{sa} proportional gain, A/V

K_{sc} flow pressure coefficient, m^5/(Nm)

K_{sd} differential coefficients in the swashplate controller

K_{sg} displacement gradient, rad/m

K_{sp} proportional coefficients in the swashplate controller

K_{ss} stiffness coefficient in the swashplate system, N/m

K_{sq} flow gain coefficient, m^2/s

K_{sv} servo value gain, m/A

m_f total mass in the fin angle system, kg

m_s equivalent mass in the swashplate system, kg

V_{st} total volume in the swashplate system, m^3

x_1, x_2, x_3 fin angle, angular rate, angular acceleration

x_{sv} spool displacement, m

$\overline{x}$ states increment

$\overline{x}_e$ extended states increment

y output of the fin angle system

y_f piston rod displacement in the fin angle system, m

y_s piston rod displacement in the swashplate system, m

α_f fin angle, rad

α_{fr} fin angle command, rad

α_s swashplate angle, rad

α_{sL} the lower limit of swashplate angle, rad

α_{sU} the upper limit of swashplate angle, rad

α_{sr} swashplate command, rad

α_{fr}^* planned fin angle command, rad

$\overline{\alpha}_{sL}, \overline{\alpha}_{sU}$ increments of α_{sL}, α_{sU}

β_{cs} incomplete differential coefficient in the swashplate controller

β_{cf} incomplete differential coefficient in fin angle controller

β_{pe} effective bulk modulus in the fin angle system, N/m^2

β_{se} effective bulk modulus in the swashplate system, N/m^2

η control sequences

μ disturbance compensation in the control command

ω_{sn} servo valve natural frequency, rad/s

ω_{fr}^* planned angular rate command

ξ_{sn} non-dimensional damping ratio